Journal of Solution Chemistry (2023) 52:447–466
https://doi.org/10.1007/s10953-022-01245-0

A Thermodynamic Model for Nd(III)–Sulfate Interaction at High Ionic Strengths and Elevated Temperatures: Applications to Rare Earth Element Extraction

Yongliang Xiong[1] · Guangping Xu[2] · Yifeng Wang[1]

Received: 18 June 2022 / Accepted: 28 December 2022 / Published online: 18 February 2023
© The Author(s), under exclusive licence to Springer Science+Business Media, LLC, part of Springer Nature 2023

Abstract
Neodymium (Nd), a rare earth element (REE), is critical to numerous industries. Neodymium can be extracted from ore concentrates, waste materials, or recycled materials such as recycled Nd-Fe-B permanent magnets. In a standard process, concentrated sulfuric acid (H_2SO_4) is used as an extraction/leaching agent. Therefore, knowledge of Nd(III)–sulfate interaction at high ionic strengths is important for optimization of the extraction process. In addition, sulfate is also a major species in natural surface waters and present in nuclear waste streams. Nd(III) has been used a chemical analog to trivalent actinides in nuclear waste research and development. Consequently, knowledge of Nd(III)-sulfate interactions is also impactful to the field of nuclear waste management. In this study, we have developed a thermodynamic model that can describe the interaction of Nd(III) with sulfate to ionic strengths up to ~ 16.5 mol·kg^{-1} and to temperatures up to 100 °C. The model adopts the Pitzer formulation to describe activity coefficients of aqueous species. This model can be used to design and optimize a chemical process for REE recovery from ore concentrates, recycled materials, and acid mine drainage (AMD) and to understand the mobility of REEs and actinides in the environment.

Keywords Pitzer model · Extraction of rare earth elements from acid mine drainage · Nuclear waste management · Neodymium sodium double sulfate salts · Neodymium potassium double sulfate salts · Recycle of Nd-Fe-B permanent magnets

1 Introduction

Rare earth elements (REEs) are critical to numerous high technology devices, including computer hard disks, smart phones, digital cameras, fluorescent and light-emitting-diode (LED) lights, flat screen televisions, computer monitors, and electronic displays. In

✉ Yongliang Xiong
yxiong@sandia.gov

[1] Department of Nuclear Waste Disposal Research and Analysis, Sandia National Laboratories (SNL), 1515 Eubank Boulevard SE, Albuquerque, NM 87123, USA

[2] Department of Geochemistry, Sandia National Laboratories (SNL), 1515 Eubank Boulevard SE, Albuquerque, NM 87123, USA

addition, the chemical behavior of lanthanides such as Pr(III) and Nd(III) is very similar to those of trivalent actinides, which are important to nuclear waste management. Pr(III) is considered to be an excellent analog to Pu(III) [1], and Nd(III) a good analog to Am(III) and Cm(III) (e.g., [2]).

Neodymium is usually extracted from various resources such as ore concentrates, recycled permanent Nd-Fe-B magnets, and rare earth powder waste by using concentrated H_2SO_4 (e.g., [3–14]), or sulfate-dominated solutions (e.g., [15–18]). For instance, ore concentrates and rare earth powder waste are roasted with H_2SO_4 at elevated temperatures up to 180 °C for extraction of REE including Nd (e.g., [8, 19]). In addition, REE including Nd is also recovered from fluorescent lamps and nickel-metal hydride batteries in forms ranging from AA batteries to the batteries used in all-electric plug vehicles and hybrid electric vehicles, using sulfuric acid as a leaching agent at temperatures up to 120 °C [20–22]. Therefore, knowledge of Nd(III)–sulfate interaction in a wide range of ionic strengths is important to optimize the extraction process.

Similar knowledge for such interactions is also required for nuclear waste management, because actinides are present in waste streams and sulfate is present either in waste streams or in the groundwaters associated with geological repositories, or sulfate can be from both of the above sources. For instance, in the low level and intermediate level radioactive sulfate liquid waste (LLW and ILW) in Spain, the waste streams are very rich in sulfate, containing up to 2.1 mol·dm^{-3} of sulfate [23]. In USA nuclear waste management programs, the sulfate concentrations in the brines at the Waste Isolation Pilot Plant (WIPP), a U.S. Department of Energy geological repository for the permanent disposal of defense-related transuranic (TRU) waste, are 0.203 mol·kg^{-1} and 0.187 mol·kg^{-1} in the Generic Weep Brine (GWB) and Energy Research and Development Administration Well 6 (ERDA-6) [24], respectively. In our previous studies, we performed a preliminary investigation of Nd(III))/Am(III)–sulfate interactions, primarily in the field of nuclear waste management [25–27].

Acid mine drainage (AMD) had been reported to be enriched with both REEs and sulfate (e.g., [28–32]). For example, the concentrations of Nd(III) in AMD from the Wishiowka mining area in south-central Poland range from 1.577 to 4.288 ppm [31]. Sulfate concentrations in AMD are usually high. For instance, the sulfate concentrations in the AMD from the Wishiowka mining area are up to ~ 3.4 mol·dm^{-3} [31]. Therefore, knowledge of Nd(III)–sulfate interaction at high ionic strengths is also applicable to the extraction of REE from AMD.

We have developed a thermodynamic model for describing the interaction of Nd(III) with sulfate to high ionic strengths up to ~ 16.5 mol·kg^{-1} over the temperature range from 0 to 100 °C in this work. In the model developed, we use the Pitzer model to calculate activity coefficients of aqueous species. The model is then validated by experimental data not used in the model development. We expect more environmentally friendly extraction technologies to emerge for REE extraction. The model presented in this work can serve as a benchmark for the future technologies.

The experimental data used for the model development in this work for the interactions of Nd(III) with sulfate are mainly based on the solubility data of $Nd_2(SO_4)_3{\cdot}8H_2O$ in H_2SO_4 solutions from [3]. In addition to knowledge of the interactions of Nd(III) with sulfate, understanding of the solubility of $Nd_2(SO_4)_3{\cdot}8H_2O$ is also important, as $Nd_2(SO_4)_3{\cdot}8H_2O$ is the solubility-limiting phase in the extraction processes using concentrated H_2SO_4. The experimental data from [3] cover the temperature range from 0 to 80 °C and the H_2SO_4 concentration range up to ~ 5.5 mol·kg^{-1} with the corresponding ionic strengths up to ~ 16.5 mol·kg^{-1}. Those conditions are expected in the extraction process.

Besides the solubility constants of $Nd_2(SO_4)_3{\cdot}8H_2O$ applicable to the extraction process, the solubility constants of other Nd(III)-sulfate phases relevant to the extraction such as $NaNd(SO_4)_2{\cdot}H_2O$, $KNd(SO_4)_2{\cdot}H_2O$, and $K_6Nd_4(SO_4)_9{\cdot}8H_2O$ are also obtained by using the model established in this study.

2 Methods

In this study, the standard state for a solid phase is defined as its pure phase with unity of activity at the temperature and pressure of interest. Similarly, the standard state of the solvent in an aqueous solution is pure water at the temperature and pressure of interest. The standard state for an aqueous solute is a hypothetical 1 molal ($mol{\cdot}kg^{-1}$) solution referred to infinite dilution at the temperature and pressure of interest.

The computer code EQ3/6 Version 8.0a [33, 34] is employed as the modeling platform. The objective of the modeling is to minimize the difference between experimental and model predictions by adjusting model parameters. A similar modeling approach for elevated temperatures can be found in [35–37].

In the modeling, experimental data from the literature are used to generate EQ3/6 input files in the first step. In the second step, the values of the targeted parameter (e.g., $\log_{10} K$ and Pitzer parameters) are varied until the difference between experimental values (e.g., $m_{\Sigma Nd(III)}$) and model predictions is minimized. In the third step, the final selected value for the targeted parameter is verified to see how it reproduces experimental data.

The EQ3/6 database, DATA0.FM2 [38–40], is used as the basis for modeling. The interactions for major ions in the database are based on the model from [41], which is modified with the addition of dissociation constants of sulfuric acid at high temperatures and 0 °C. The dissociation constant of sulfuric acid at high temperatures and 0 °C along with ionization constants of water at the corresponding temperatures is taken from the EQ3/6 database DATA0.YPF [42]. The usage of the model from [41] for major ions takes into consideration the wide application of this database in scientific community. In the major ion model from [41], the associations of sodium and potassium ions with sulfate were not explicitly considered. Instead, they were absorbed by the respective Pitzer parameters for $Na^+ - SO_4^{2-}$ and $K^+ - SO_4^{2-}$ interactions. Truesdell and Hostetler [43] and Pokrovski et al. [44], respectively, determined the association constants of KSO_4^- and $NaSO_4^-$. In this study, the associations constants of $NaSO_4^-$ and KSO_4^- are not included in order to be consistent with the model from [41].

The database for major ion interactions from [41] is at 25 °C. When this database is used for modeling, it is assumed that interaction parameters for major ions are constant over the temperature range from 25 to 100 °C. This assumption is based on the observation that the Pitzer interaction parameters do not change significantly over a narrow range of temperature. For instance, the temperature derivative of $\beta^{(1)}$ for H^+–HSO_4^- is small over the temperature range from 25 to 100 °C, i.e., $(\frac{\partial \beta^{(1)}}{\partial T})_P = -1.96 \times 10^{-4}$ ([45]; compiled in DATA0.YPF in [42]). Similarly, the temperature derivative of $\beta^{(0)}$ for $Na^+ - HSO_4^-$ is also small over the temperature range from 25 to 100 °C, i.e., $(\frac{\partial \beta^{(0)}}{\partial T})_P = -3.47 \times 10^{-5}$ ([45]; compiled in DATA0.YPF in [42]). The Specific ion Interaction Theory (SIT) is considered as a simplified Pitzer formalism (e.g., [46]). The temperature derivatives of the SIT interaction coefficients ε for major ions, for instance, Na^+–Cl^-, are also small over the temperature range from 25 to 100 °C, e.g., $(\frac{\partial \varepsilon}{\partial T})_P = -5.2 \times 10^{-5}$ for Na^+–Cl^- [47].

Additionally, the database DATA0.YPF from [42, 48, 49] is also applied in the companion and alternate modeling. In this database, the Pitzer interaction parameters are valid to high temperatures up to 250 °C. As detailed in the following section on the results, the parameters obtained by using both databases are close.

The uncertainties reported in this study are two standard deviations (2σ). Error propagations are calculated based on uncertainties associated with regression and equilibrium constants in the model.

The stability constants for $NdSO_4^+$ and $Nd(SO_4)_2^-$ in our model at 25 °C are based on the experimental data, whereas at other temperatures they are extrapolated values. The extrapolated values are obtained using the one-term isocoulombic principal [50], and $AlSO_4^+$, and $Al(SO_4)_2^-$ from [51, 52] as model substances as described below. The choice of $AlSO_4^+$ and $Al(SO_4)_2^-$ as the model substances is because they are the same like-charged species as $NdSO_4^+$ and $Nd(SO_4)_2^-$ on one hand and their values at the temperatures of interest are experimentally well determined on the other hand.

The formation of $NdSO_4^+$ can be expressed as

$$Nd^{3+} + SO_4^{2-} \rightleftharpoons NdSO_4^+ \tag{1}$$

using $AlSO_4^+$ as a model substance,

$$Al^{3+} + SO_4^{2-} \rightleftharpoons AlSO_4^+ \tag{2}$$

The combination of Equations 1 and 2 leads to the following ideal isocoulombic reaction,

$$Nd^{3+} + AlSO_4^+ \rightleftharpoons Al^{3+} + NdSO_4^+ \tag{3}$$

Therefore, the equilibrium constants at the temperatures of interest for the reaction in Eq. 3 can be calculated based on the one-term isocoulombic principal. The one-term isocoulombic principal for extrapolation of equilibrium constants for aqueous reactions is based on the observation that the temperature function of the change in free energy (i.e., $\Delta_r G$) for a well-balanced isocoulombic reaction has a slope of almost zero, as the entropies and heat capacities of an isocoulombic reaction cancel out or are close to zero [50]. Accordingly, the stability constants for $NdSO_4^+$ at the respective temperatures can be retrieved when Eq. 3 is combined with Eq. 2 having the equilibrium constants at the respective temperatures.

Similarly, using $Al(SO_4)_2^-$ as the model substance, the following ideal isocoulombic reaction can be cast,

$$Nd^{3+} + Al\left(SO_4\right)_2^- \rightleftharpoons Al^{3+} + Nd\left(SO_4\right)_2^- \tag{4}$$

Based on Eq. 4, the stability constants for $Nd\left(SO_4\right)_2^-$ at various temperatures other than 25 °C can be obtained.

Our extrapolated values have three significant numbers along with estimated uncertainties, the same number of significant numbers as original experimental data in [51, 52]. However, only two significant numbers are reported in Ridley et al. [51] for their values that are smoothed for temperature and ionic strength.

It should be noted that Wood [53, 54] provided the formation constants for both $NdSO_4^+$ and $Nd\left(SO_4\right)_2^-$ from 25 to 350 °C, which can be alternatively used in our model. Migdisov et al. [55] and Migdisov and William-Jones [56] subsequently performed the experimental

studies to determine the formation constants to 250 °C, which are in excellent agreement with those from Wood [53, 54]. However, in order to be consistent with the formation constants and the associated Pitzer parameters at 25 °C from [57, 58] utilized in the database DATA0.FM2 [38–40] for modeling, we choose to use the one-term isocoulombic approach to get the formation constants at elevated temperatures for the internal consistency. The extrapolated values at elevated temperatures are in reasonable agreement with those from [53–56]. For instance, the extrapolated $\log_{10} K_1$ and $\log_{10} K_2$ (step-wise formation constants) at 100 °C are 4.02 and 2.26, respectively, in favorable comparison with 4.77 and 2.27 from [53, 54], respectively, and 4.32 and 2.43 from [55, 56].

It should be emphasized that both $NdSO_4^+$ and $Nd(SO_4)_2^-$ are incorporated in our model at all of the temperatures. It is worth noting that Rai et al. [59] developed a thermodynamic model to describe Nd(III)/Am(III)–sulfate interactions at 25 °C. In their model, they did not explicitly consider the complexation of Nd(III)/Am(III) with sulfate to form $Nd(SO_4)_2^+/AmSO_4^+$ and $Nd(SO_4)_2^-/Am(SO_4)_2^-$. Instead, they used $\beta^{(2)}$ for the interaction parameters of $Nd^{3+}/Am^{3+} - SO_4^{2-}$, which implies the formation of $NdSO_4^+/AmSO_4^+$ in dilute range. In the Pitzer model, $\beta^{(2)}$ is defined by the following equation,

$$\frac{2\beta_{MX}^{(2)}}{\alpha_2^2 \times I_m} \times [1 - (1 + \alpha_2\sqrt{I_m} - \frac{1}{2} \times \alpha_2^2 \times I_m)e^{-\alpha_2\sqrt{I_m}}] \quad (5)$$

where α_2 usually has a value of 12, and I_m is an ionic strength on a molal scale. Equation 5 indicates that the contributions from $\beta^{(2)}$ (i.e., the association of Nd^{3+}/Am^{3+} with SO_4^{2-}, $NdSO_4^+/AmSO_4^+$) rapidly diminish with increasing ionic strength. As high ionic strengths up to ~ 16.5 mol·kg^{-1} are expected to be frequently encountered in industrial processes, the reliance on $\beta^{(2)}$ to account for the association of Nd^{3+} with SO_4^{2-} in high ionic strength range does not work well. Indeed, Rai et al. [59] mentioned that their model is valid only in low sulfate concentrations, limited to ≤ 0.5 mol·kg^{-1}.

Das et al. [60] also developed a thermodynamic model to describe the interactions of REE with sulfate in the framework of mixed-solvent electrolyte (MSE). In their model, they adopted $REESO_4^+$, but excluded $REE(SO_4)_2^-$. As both $REE(SO_4)_2^-$ and its analog $Cm(SO_4)_2^-$ are important in high sulfate concentrations, especially at elevated temperatures (e.g., [53–56, 61, 62]), the neglect of $REE(SO_4)_2^-$ is neither ideal nor reflects what really happens in industrial processes with high sulfate concentrations. In such high concentrations of sulfate, $REE(SO_4)_2^-$ makes important contributions to total REE concentrations.

3 Results: Thermodynamic Model

The parameters obtained in this study are listed in Tables 1, 2, 3, 4, 5, 6. In Table 1, the key parameters at 0 °C and 25 °C are presented. For the binary interactions of Nd^{3+}–SO_4^{2-}, Nd^{3+}–HSO_4^-, and $NdSO_4^+$–HSO_4^-, we found that the values at 25 °C can be applied at 0 °C, and we therefore evaluated the theta parameter (θ) for H^+–$NdSO_4^+$ only. The theta parameter for Nd^{3+}–H^+ has been independently evaluated in [1], which is compatible with the current model. The theta parameter for H^+–$NdSO_4^+$ is kept at the same value as evaluated at 0 °C. Note that $\beta^{(1)}$ for Nd^{3+}–HSO_4^-, $NdSO_4^+$–HSO_4^-, and $NdSO_4^+$–SO_4^{2-} are set to 5.22, 0.29, and 1.74, respectively, according to the paradigm of Choppin et al. [63] by setting a value to an average value for a specific charge interaction group (e.g., 3:1/1:3, 1:1, and 1:2/2:1 interactions).

Table 1 Key parameters describing solubility of $Nd_2(SO_4)_3{\cdot}8H_2O$ in H_2SO_4 solutions at 0 °C and 25 °C

Pitzer binary parameters				
Species, *i*	Species, *j*	$\beta^{(0)}$	$\beta^{(1)}$	C^{ϕ}
Nd^{3+}	SO_4^{2-}	1.792[a]	15.04[a]	0.6[a]
Nd^{3+}	HSO_4^-	1.410[b,c]	5.22[b,c]	0
$NdSO_4^+$	HSO_4^-	0.1391[b], 0.1325[c] (25 °C only)	0.29[b,c]	0
$NdSO_4^+$	SO_4^{2-}	0.9425[b] (25 °C only), 0.9896[c] (25 °C only)	1.74[b,c]	0

Pitzer mixing parameters				
Species, *i*	Species, *j*	Species, *k*	θ_{ij}	Ψ_{ijk}
Nd^{3+}	H^+	SO_4^{2-}/HSO_4^-	0 (0 °C), 0.3051(25 °C)[b,c,d]	0.0
H^+	$NdSO_4^+$		0.0097[b,c]	

Equilibrium constants at infinite dilution for dissolution reaction of $Nd_2(SO_4)_3{\cdot}8H_2O$, and dissociation reactions of $NdSO_4^+$ and $Nd(SO_4)_2^-$	
Reactions	$\log_{10} K^0$
$Nd_2(SO_4)_3{\cdot}8H_2O(cr) \rightleftharpoons 2Nd^{3+} + 3SO_4^{2-} + 8H_2O(l)$	–9.00 ± 0.42 (0 °C)[e], –9.99 ± 0.21 (25 °C)[b,c]
$NdSO_4^+ \rightleftharpoons Nd^{3+} + SO_4^{2-}$	–2.85 ± 0.30 (0 °C)[e], –3.25 ± 0.15 (25 °C)[b,c]
$Nd(SO_4)_2^- \rightleftharpoons Nd^{3+} + 2SO_4^{2-}$	–2.91 ± 0.30 (0 °C)[e], –3.70 ± 0.15 (25 °C) [b,c]

Unless otherwise noted, values are from this work. The designation of "cr" for a solid phase refers to its crystalline state.

[a]Values at 25°C from the thermodynamic database, DATA0.FM2 [38–40] (using Am(III) as an analog to Nd(III), which originated from [57, 58]. As noted in text, the same values for $\beta^{(1)}$ and C^{ϕ} are used for other temperatures.

[b]Applied to the database with Pitzer parameters for major ions at 25°C from [41]

[c]Applied to the database with Pitzer parameters for major ions at high temperatures up to 250°C from [42]

[d]From Ref. [1]

[e]Extrapolated values, using the one-term isocoulombic principal [50], and $AlSO_4^+$, and $Al(SO_4)_2^-$ from [51, 52] as model substances. In the following tables, this footnote will be simplified as "Using isocoulombic extrapolation" to avoid the repetition.

In Table 2, the key parameters for the interactions at 40 °C are tabulated. For the interaction of Nd^{3+}–SO_4^{2-}, $\beta^{(1)}$ and C^{ϕ} are the same as those at 25 °C, meaning that they are constant, and only $\beta^{(o)}$ is changed. For the interactions of Nd^{3+}–HSO_4^- and $NdSO_4^+$–HSO_4^-, $\beta^{(1)}$ is a constant and only $\beta^{(o)}$ is a variable. For the interaction of $NdSO_4^+$–SO_4^{2-}, both $\beta^{(o)}$ and $\beta^{(1)}$ are constant.

In Table 3, the key parameters for describing the interactions at 60 °C are tabulated. Similar to the descriptions for the parameters at 40 °C, for the interaction of Nd^{3+}–SO_4^{2-}, $\beta^{(1)}$ and C^{ϕ} are constant, and only $\beta^{(o)}$ is changed. For the interaction of Nd^{3+}–HSO_4^-, $\beta^{(1)}$ is constant, and only $\beta^{(o)}$ is changed. For the interaction of $NdSO_4^+$–HSO_4^-, $\beta^{(1)}$ is also constant, and only $\beta^{(o)}$ is changed. For the interaction of $NdSO_4^+$–SO_4^{2-}, both $\beta^{(o)}$ and $\beta^{(1)}$ are constant.

The key parameters for describing the interactions at 80 °C are listed in Table 4. Similar to the descriptions for the parameters at 40 °C and 60 °C, for the interaction of Nd^{3+}–SO_4^{2-},

Table 2 Key parameters describing solubility of $Nd_2(SO_4)_3{\cdot}8H_2O$ in H_2SO_4 solutions at 40 °C

Pitzer binary parameters				
Species, *i*	Species, *j*	$\beta^{(0)}$	$\beta^{(1)}$	C^{ϕ}
Nd^{3+}	SO_4^{2-}	1.908[a] 2.000[b]	15.04[a,b]	0.6[a,b]
Nd^{3+}	HSO_4^-	1.830[a] 1.825[b]	5.22[a,b]	0
$NdSO_4^+$	HSO_4^-	0.1530[a] 0.1525[b]	0.29[a,b]	0
$NdSO_4^+$	SO_4^{2-}	0.9425[a,b]	1.74[a,b]	

Pitzer mixing parameters				
Species, *i*	Species, *j*	Species, *k*	θ_{ij}	Ψ_{ijk}
Nd^{3+}	H^+	SO_4^{2-}/HSO_4^-	0	0.0

Equilibrium constants at infinite dilution for dissolution reaction of $Nd_2(SO_4)_3{\cdot}8H_2O$, and dissociation reactions of $NdSO_4^+$ and $Nd(SO_4)_2^-$

Reactions	$\log_{10} K^0$
$Nd_2(SO_4)_3{\cdot}8H_2O(cr) \rightleftharpoons 2Nd^{3+} + 3SO_4^{2-} + 8H_2O(l)$	-10.73 ± 0.30[a,b]
$NdSO_4^+ \rightleftharpoons Nd^{3+} + SO_4^{2-}$	-3.30 ± 0.13[a,b,c]
$Nd(SO_4)_2^- \rightleftharpoons Nd^{3+} + 2SO_4^{2-}$	-4.03 ± 0.27[a,b,c]

[a]Identical to footnote b in Table 1

[b]Identical to footnote c in Table 1

[c]Using the isocoulombic extrapolation

$\beta^{(1)}$ and C^{ϕ} are constant, and only $\beta^{(o)}$ is a variable. For the interaction of Nd^{3+}–HSO_4^-, $\beta^{(1)}$ is constant, and only $\beta^{(o)}$ is changed. For the interaction of $NdSO_4^+$–HSO_4^-, $\beta^{(1)}$ is also constant, and only $\beta^{(o)}$ is changed. For the interaction of $NdSO_4^+$–SO_4^{2-}, both $\beta^{(o)}$ and $\beta^{(1)}$ are constant.

In Tables 1, 2, 3, the Pitzer parameters obtained using the database DATA0.YPF [42] with the high temperature Pitzer parameters for major ions are also tabulated. It is apparent that the Pitzer parameters obtained using both databases are close. At 80 °C, they are identical (Table 4). Therefore, for sake of simplicity, the regression equations below are established using the Pitzer parameters obtained using the database from [41], and they can be approximately applied to the database DATA0.YPF from [42].

The parameters describing the interactions of Nd^{3+} and $NdSO_4^+$ with sulfate at different temperatures are plotted in Fig. 1. According to the variation of the parameters with temperature, the model parameters are extrapolated to 100 °C (Table 5). The key parameters for describing the interactions at 100 °C are listed in Table 5. Similar to the descriptions for the parameters at 40 °C, 60 °C, and 80 °C for the interaction of Nd^{3+}–SO_4^{2-}, $\beta^{(1)}$ and C^{ϕ} are constant and the same as other temperatures, and only $\beta^{(o)}$ is changed. The $\beta^{(o)}$ for Nd^{3+}–SO_4^{2-} at 100 °C is calculated from the following regression equation,

Table 3 Key parameters describing solubility of $Nd_2(SO_4)_3{\cdot}8H_2O$ in H_2SO_4 solutions at 60 °C

Pitzer binary parameters				
Species, *i*	Species, *j*	$\beta^{(0)}$	$\beta^{(1)}$	C^{ϕ}
Nd^{3+}	SO_4^{2-}	1.975[a,b]	15.04[a,b]	0.6[a,b]
Nd^{3+}	HSO_4^-	2.2025[a] 2.3126[b]	1.74[a,b]	0
$NdSO_4^+$	HSO_4^-	0.1825[a,b]	0.29[a,b]	0
$NdSO_4^+$	SO_4^{2-}	0.9425[a,b]	1.74[a,b]	
Pitzer mixing parameters				
Species, *i*	Species, *j*	Species, *k*	θ_{ij}	Ψ_{ijk}
Nd^{3+}	H^+	SO_4^{2-}/HSO_4^-	0	0.0
Equilibrium constants at infinite dilution for dissolution reaction of $Nd_2(SO_4)_3{\cdot}8H_2O$, and dissociation reactions of $NdSO_4^+$ and $Nd(SO_4)_2^-$				
Reactions				$\log_{10} K^0$
$Nd_2(SO_4)_3{\cdot}8H_2O(cr) \rightleftharpoons 2Nd^{3+} + 3SO_4^{2-} + 8H_2O(l)$				-11.18 ± 0.22[a,b]
$NdSO_4^+ \rightleftharpoons Nd^{3+} + SO_4^{2-}$				-3.36 ± 0.14[a,b,c]
$Nd(SO_4)_2^- \rightleftharpoons Nd^{3+} + 2SO_4^{2-}$				-4.53 ± 0.17[a,b,c]

[a]Identical to footnote b in Table 1

[b]Identical to footnote c in Table 1

[c]Using the isocoulombic extrapolation

Table 4 Key parameters describing solubility of $Nd_2(SO_4)_3{\cdot}8H_2O$ in H_2SO_4 solutions at 80 °C

Pitzer binary parameters				
Species, *i*	Species, *j*	$\beta^{(0)}$	$\beta^{(1)}$	C^{ϕ}
Nd^{3+}	SO_4^{2-}	1.987[a,b]	15.04[a,b]	0.6[a,b]
Nd^{3+}	HSO_4^-	2.355[a,b]	1.74[a,b]	0
$NdSO_4^+$	HSO_4^-	0.205[a,b]	0.29[a,b]	0
$NdSO_4^+$	SO_4^{2-}	0.9425[a,b]	1.74[a,b]	
Pitzer mixing parameters				
Species, *i*	Species, *j*	Species, *k*	θ_{ij}	Ψ_{ijk}
Nd^{3+}	H^+	SO_4^{2-}/HSO_4^-	0	0.0
Equilibrium constants at infinite dilution for dissolution reaction of $Nd_2(SO_4)_3{\cdot}8H_2O$, and dissociation reactions of $NdSO_4^+$ and $Nd(SO_4)_2^-$				
Reactions				$\log_{10} K^0$
$Nd_2(SO_4)_3{\cdot}8H_2O(cr) \rightleftharpoons 2Nd^{3+} + 3SO_4^{2-} + 8H_2O(l)$				-11.80 ± 0.22[a,b]
$NdSO_4^+ \rightleftharpoons Nd^{3+} + SO_4^{2-}$				-3.57 ± 0.14[a,b,c]
$Nd(SO_4)_2^- \rightleftharpoons Nd^{3+} + 2SO_4^{2-}$				-5.25 ± 0.17[a,b,c]

[a]Identical to footnote b in Table 1

[b]Identical to footnote c in Table 1

[c]Using the isocoulombic extrapolation

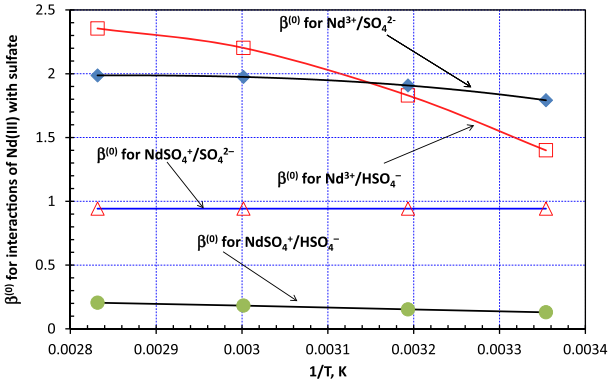


Fig. 1 A plot showing the Pitzer parameters [$\beta^{(0)}$] describing the interactions of Nd^{3+} and $NdSO_4^+$ with sulfate as a function of reciprocal temperature

Table 5 Key parameters describing solubility of $Nd_2(SO_4)_3{\cdot}8H_2O$ in H_2SO_4 solutions at 100 °C

Pitzer binary parameters				
Species, *i*	Species, *j*	$\beta^{(0)}$	$\beta^{(1)}$	C^{ϕ}
Nd^{3+}	SO_4^{2-}	1.9738[a,b]	15.04[a,b]	0.6[a,b]
Nd^{3+}	HSO_4^-	2.7099[a,b]	1.74[a,b]	0
$NdSO_4^+$	HSO_4^-	0.2278[a,b]	0.29[a,b]	0
$NdSO_4^+$	SO_4^{2-}	0.9425[a,b]	1.74[a,b]	
Pitzer mixing parameters				
Species, *i*	Species, *j*	Species, *k*	θ_{ij}	Ψ_{ijk}
Nd^{3+}	H^+	SO_4^{2-}/HSO_4^-	0	0.0
Equilibrium constants at infinite dilution for dissolution reaction of $Nd_2(SO_4)_3{\cdot}8H_2O$, and dissociation reactions of $NdSO_4^+$ and $Nd(SO_4)_2^-$				
Reactions				$\log_{10} K^0$
$Nd_2(SO_4)_3{\cdot}8H_2O(cr) \rightleftharpoons 2Nd^{3+} + 3SO_4^{2-} + 8H_2O(l)$				−12.32 ± 0.25[a,b]
$NdSO_4^+ \rightleftharpoons Nd^{3+} + SO_4^{2-}$				−4.05 ± 0.14[a,b,c]
$Nd(SO_4)_2^- \rightleftharpoons Nd^{3+} + 2SO_4^{2-}$				−6.31 ± 0.16[a,b,c]

Unless otherwise noted, values are extrapolated from temperature dependences of parameters evaluated from other temperatures.

[a]Identical to footnote b in Table 1

[b]Identical to footnote c in Table 1

[c]Using the isocoulombic extrapolation

$$\beta^{(o)} = -5.47823 \times 10^8 \left(\frac{1}{T}\right)^3 + 4.17393 \times 10^6 \left(\frac{1}{T}\right)^2 - 1.04337 \times 10^4 \left(\frac{1}{T}\right) + 1.05022 \times 10 \left(R^2 = 1.00\right) \quad (6)$$

where T is temperature in Kevin.

For the interaction of Nd^{3+}–HSO_4^- at 100 °C, $\beta^{(1)}$ is constant and is the same as the values at other temperatures, and only $\beta^{(o)}$ is changed. The $\beta^{(o)}$ for Nd^{3+}–HSO_4^- at 100 °C is calculated from the following regression equation,

$$\beta^{(o)} = -1.83743 \times 10^4 \left(\frac{1}{T}\right) + 7.63405 \left(R^2 = 0.97\right) \tag{7}$$

For the interaction of $NdSO_4^+$–HSO_4^- at 100 °C, $\beta^{(1)}$ is the same as the values at other temperatures and is constant, and only $\beta^{(o)}$ is changed. The $\beta^{(o)}$ for $NdSO_4^+$—HSO_4^- at 100 °C is calculated from the following regression equation,

$$\beta^{(o)} = -1.44774 \times 10^2 \left(\frac{1}{T}\right) + 0.61573 \left(R^2 = 1.00\right) \tag{8}$$

For the interaction of $NdSO_4^+$–SO_4^{2-} at 100 °C, both $\beta^{(o)}$ and $\beta^{(1)}$ are constant values as at other temperature.

The solubility product constant ($\log_{10} K_{sp}$) for $Nd_2(SO_4)_3{\cdot}8H_2O$ at 100 °C is calculated from the following regression equation,

$$\log_{10} K_{sp} = 3.377001 \times 10^3 \left(\frac{1}{T}\right) - 21.37537 \left(R^2 = 0.99\right) \tag{9}$$

The above regression equations can be applied for interpolation of our model at other temperatures in the range of 25–100 °C. In addition, it is expected that our model as summarized in Table 6 could be further extrapolated to 125 °C. This is based on the fact that the temperature grid for the stability constants of $NdSO_4^+$ and $Nd(SO_4)_2^-$ is supported by the temperature limit of the model substances of $AlSO_4^+$ and $Al(SO_4)_2^-$, which is valid to 125 °C [51, 52].

4 Model Verification and Validation

4.1 Model Verification and Validation Tests

In the following, we first perform verification tests by comparing solubilities of $Nd_2(SO_4)_3{\cdot}8H_2O$ as a function of H_2SO_4 concentration predicted by the model with the experimental data used in the model development. Then, we conduct the validation tests by comparing the predicted solubilities of $Nd_2(SO_4)_3{\cdot}8H_2O$ as a function of H_2SO_4 concentrations with the experimental data that were not used for the model development.

Figure 2 shows verification and validation tests at 0 °C and 25 °C. It shows that the model reproduces reasonably well the experimental data from [3] used for the model development. The experimental data that are not used for the model development and utilized for the validation tests include the data at 0–0.2 °C [64], at 11–15 °C [64], at 25 °C [65–68], and at 30.4 °C [64]. Figure 2 shows that the model-predicted values are in close agreement with the model-independent experimental data, validating our model at 0 °C and 25 °C.

Figure 3 displays the verification and validation tests at 40 °C and 60 °C. It shows that the model-predicted values at 40 °C and 60 °C are close to each other, and the model reproduces the experimental data used for the model development. The experimental data for the validation tests of the model at 40 °C include those from [65] at 40 °C and from [64] at 46.4 °C. The data for the validation tests of the model at 60 °C include those from [69] at 50 °C, from [65] at 55 °C, from [64] at 59 °C, and from [67] at 64 °C. The model-predicted values are in reasonable agreement with those model-independent experimental data.

Table 6 Summary of key parameters describing the interactions of Nd(III) with sulfate at elevated temperatures from 40 to 100 °C (unless otherwise noted, values are from this work)

Pitzer binary parameters

Species, *i*	Species, *j*	$\beta^{(0)}$	$\beta^{(1)}$	C^{ϕ}
Nd^{3+}	SO_4^{2-}	Temperature-dependent[a,b], See Eq. 1 in the footnote	15.04 [a,b]	0.6[a,b]
Nd^{3+}	HSO_4^-	Temperature-dependent[a,b], See Eq. 2 in the footnote	5.22[a,b]	0
$NdSO_4^+$	HSO_4^-	Temperature-dependent[a,b], See Eq. 3 in the footnote	0.29[a,b]	0
$NdSO_4^+$	SO_4^{2-}	0.9425[a,b]	1.74[a,b]	0

Pitzer mixing parameters

Species, *i*	Species, *j*	Species, *k*	θ_{ij}	Ψ_{ijk}
Nd^{3+}	H^+	SO_4^{2-}/HSO_4^-	0	0.0

Equilibrium constants at infinite dilution for dissolution reaction of $Nd_2(SO_4)_3{\cdot}8H_2O$, and dissociation reactions of $NdSO_4^+$ and $Nd(SO_4)_2^-$

Reactions	$\log_{10} K^0$
$Nd_2(SO_4)_3{\cdot}8H_2O(cr) \rightleftharpoons 2Nd^{3+} + 3SO_4^{2-} + 8H_2O(l)$	–10.73 ± 0.30 (40 °C)[a,b] –11.18 ± 0.22 (60 °C)[a,b] –11.80 ± 0.22 (80 °C)[a,b] –12.33 ± 0.25 (100 °C)[a,b]
$NdSO_4^+ \rightleftharpoons Nd^{3+} + SO_4^{2-}$	–3.30 ± 0.13 (40 °C)[a,b,c] –3.36 ± 0.14 (60 °C)[a,b,c] –3.57 ± 0.14 (80 °C)[a,b,c] –4.05 ± 0.14 (100 °C)[a,b,c]
$Nd(SO_4)_2^- \rightleftharpoons Nd^{3+} + 2SO_4^{2-}$	–4.03 ± 0.27(40 °C)[a,b,c] –4.53 ± 0.17 (60 °C)[a,b,c] –5.25 ± 0.17 (80 °C)[a,b,c] –6.31 ± 0.16 (100 °C)[a,b,c]

Equation 1 $\beta^{(o)} = -5.47823 \times 10^8 \left(\frac{1}{T}\right)^3 + 4.17393 \times 10^6 \left(\frac{1}{T}\right)^2 - 1.04337 \times 10^4 \left(\frac{1}{T}\right) + 1.05022 \times 10$ $\left(R^2 = 1.00\right)$

Equation 2 $\beta^{(o)} = -1.83743 \times 10^4 \left(\frac{1}{T}\right) + 7.63405 \left(R^2 = 0.97\right)$

Equation 3 $\beta^{(o)} = -1.44774 \times 10^2 \left(\frac{1}{T}\right) + 0.61573 \left(R^2 = 1.00\right)$

[a]Identical to footnote b in Table 1

[b]Identical to footnote c in Table 1

[c]Using the isocoulombic extrapolation

Figure 4 depicts the comparisons of the model-predicted values at 80 °C and 100 °C with the experimental data. Note that the experimental data from [3] in the model development are up to 80 °C. Therefore, the model at 100 °C is based on the extrapolation of the interaction parameters and solubility product constant to 100 °C using the regression equations, as detailed in the above section (refer to Results: Thermodynamic Model). Figure 4 shows that the model at 80 °C reproduces reasonably the experimental data from [3] used in the model development. The values predicted by the model at 80 °C are in reasonable agreement with the experimental data at 75 °C [69] and at 77.6–81 °C [64], which were not used for the model development. For the model at 100 °C, there are currently no experimental data in high ionic strength range for comparison. In the low to moderate ionic

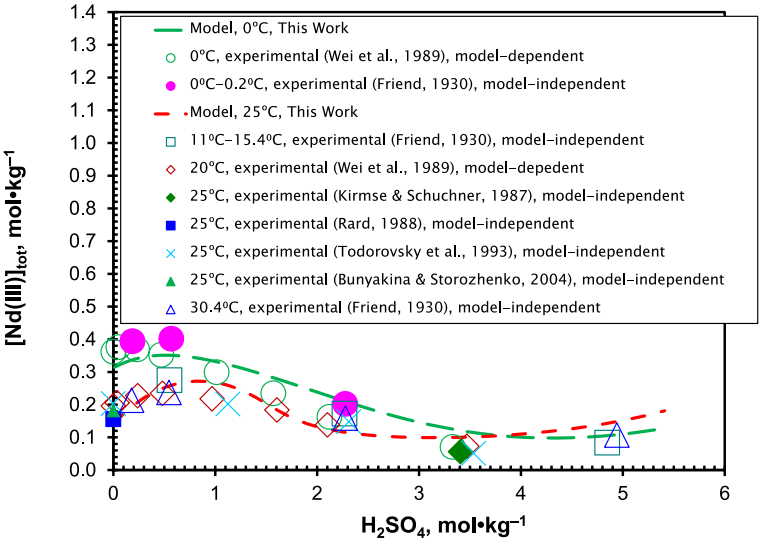


Fig. 2 Solubilities of $Nd_2(SO_4)_3{\cdot}8H_2O$ in total molality of Nd(III) at 0 °C and 25 °C as a function of concentration of H_2SO_4 predicted by the model developed in this study in comparison with the experimental data in the temperature range from 0 to 30.4 °C. In all of experiments, the solubility-controlling phase is $Nd_2(SO_4)_3{\cdot}8H_2O$ except that in Rard [66] in which $Pr_2(SO`_4)_3{\cdot}8H_2O$ is the solubility-controlling phase. Note that "model-independent" means that those experimental data were not used for the model development. Therefore, they serve as the validation tests for the model. This applies to the figures hereafter

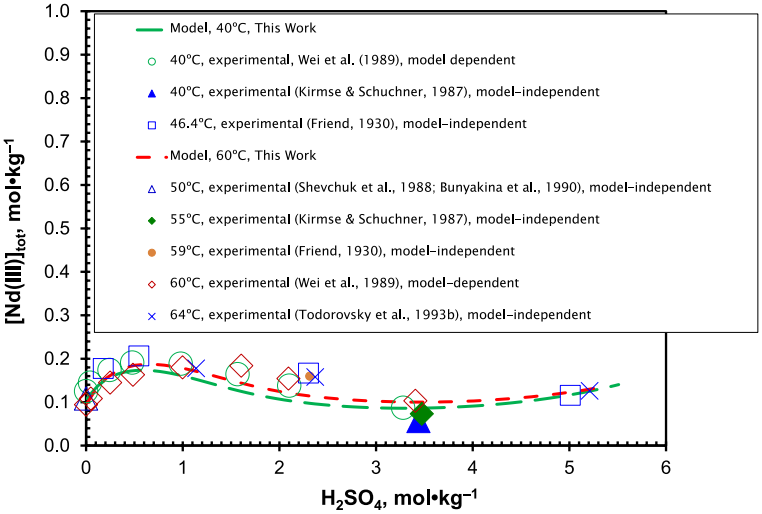


Fig. 3 Solubilities of $Nd_2(SO_4)_3{\cdot}8H_2O$ in total molality of Nd(III) at 40 °C and 60 °C as a function of concentration of H_2SO_4 predicted by the model developed in this study in comparison with the experimental data in the temperature range from 40 to 64 °C

strength range, the model-predicted values are in agreement with the experimental data at 89.6 °C [64] and at 100 °C [69], which were not utilized for the model development.

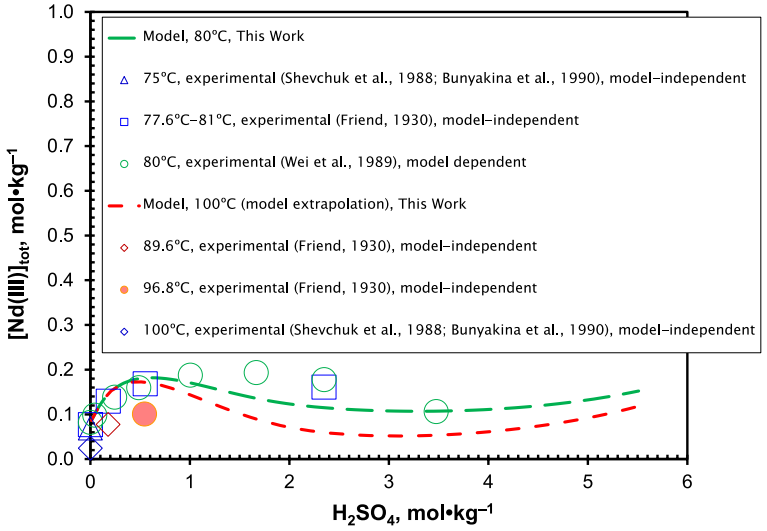


Fig. 4 Solubilities of $Nd_2(SO_4)_3{\cdot}8H_2O$ in total molality of Nd(III) at 80 °C and 100 °C as a function of concentration of H_2SO_4 predicted by the model developed in this study in comparison with the experimental data in the temperature range from 75 to 100 °C

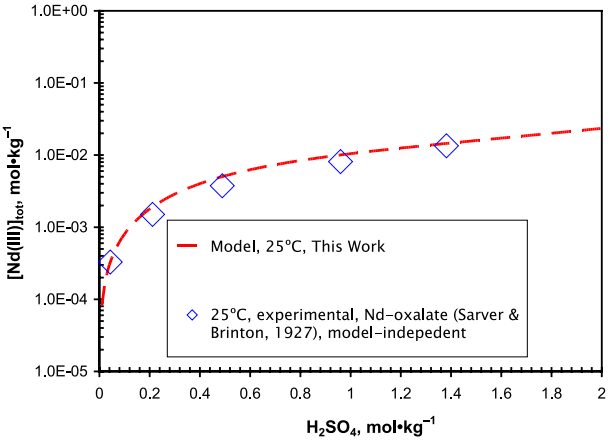


Fig. 5 Solubilities of $Nd_2(C_2O_4)_3{\cdot}10H_2O$ in total molality of Nd(III) at 25 °C as a function of concentration of H_2SO_4 predicted by the model developed in this study in comparison with the experimental data in H_2SO_4 solutions at 25 °C

However, the value at 96.8 °C at ~ 0.5 mol·kg^{-1} from [64] is significantly different from the value predicted by the model. More experimental data at 100 °C in high ionic strength range are desirable, and may help resolve the deviation.

In Fig. 5, our parameters at 25 °C are tested for the solubility of Nd-oxalate in H_2SO_4 solutions. This test is important as our parameters are evaluated from the experimental data of $Nd_2(SO_4)_3{\cdot}8H_2O$ in H_2SO_4 solutions, not from the solubility data of Nd-oxalate in H_2SO_4 solutions. In the validation test, the solubility of Nd-oxalate is calculated using the Pitzer parameters involving sulfate obtained in this study, along with the solubility constant of $Nd_2(C_2O_4)_3{\cdot}10H_2O$ from [1] and the Pitzer parameters for oxalate species from [70].

Figure 5 demonstrates that the model-predicted values are in excellent agreement with the experimental data from [71].

4.2 Model Applications

As an example of model applications, we evaluate the solubility constants for the double salts of alkali sulfates with neodymium sulfate, such as, $NaNd(SO_4)_2{\cdot}H_2O(cr)$ and $KNd(SO_4)_2{\cdot}H_2O(cr)$, based on the solubility data in a wide range of ionic strengths from literature, by using the above thermodynamic model. The solubility constants of these double salts are important to the extraction industry. In the process of extraction of REE from ore concentrates such as bastnasite, ore concentrates are first baked in H_2SO_4 solutions (e.g., [72]). Then, REE is recovered by the addition of alkali sulfates such as Na_2SO_4 to precipitate REE as double salts of alkali and REE sulfates (e.g., [72]). Similarly, REE is also recovered from leaching solutions as lanthanide-alkali double salts, when nickel-metal hydride (NiMH) batteries are recycled [73]. However, the solubility constants of these double salts are not well known. Therefore, such knowledge is of importance for extraction.

The dissolution reaction for $NaNd(SO_4)_2{\cdot}H_2O(cr)$ can be expressed as follows,

$$NaNd\left(SO_4\right)_2 \cdot H_2O(cr) \rightleftharpoons Na^+ + Nd^{3+} + 2SO_4^{2-} + H_2O(l) \tag{10}$$

Similarly, the dissolution reaction for $KNd(SO_4)_2{\cdot}H_2O(cr)$ can be expressed as the following,

$$KNd\left(SO_4\right)_2 \cdot H_2O(cr) \rightleftharpoons K^+ + Nd^{3+} + 2SO_4^{2-} + H_2O(l) \tag{11}$$

Based on the solubility data of $NaNd(SO_4)_2{\cdot}H_2O(cr)$ and $KNd(SO_4)_2{\cdot}H_2O(cr)$ in H_2SO_4 solutions at 20 °C from [74] and in K_2SO_4 solutions at 25 °C from [75], the solubility constants for $NaNd(SO_4)_2{\cdot}H_2O(cr)$ and $KNd(SO_4)_2{\cdot}H_2O(cr)$ are computed

Table 7 Solubility constants of alkali and neodymium double sulfate salts using the thermodynamic model established in this work

Reactions	$\log_{10} K^0$
$NaNd(SO_4)_2{\cdot}H_2O(cr) \rightleftharpoons Na^+ + Nd^{3+} + 2SO_4^{2-} + H_2O(l)$	–9.51 ± 0.10 (25 °C), –7.59 ± 0.20 (50 °C), –8.79 ± 0.30 (75 °C), –9.89 ± 0.45 (100 °C)
$KNd(SO_4)_2{\cdot}H_2O(cr) \rightleftharpoons K^+ + Nd^{3+} + 2SO_4^{2-} + H_2O(l)$	–8.20 ± 0.30 (25 °C), –8.22 ± 0.50 (50 °C), –8.82 ± 0.40 (75 °C), –9.93 ± 0.25 (100 °C)
$K_6Nd_4(SO_4)_9{\cdot}8H_2O(cr) \rightleftharpoons 6\,K^+ + 4Nd^{3+} + 9SO_4^{2-} + 8H_2O(l)$	–35.79 ± 1.00 (25 °C)

The $\log_{10} K_{sp}$ for $NaNd(SO_4)_2{\cdot}H_2O(cr)$ and $KNd(SO_4)_2{\cdot}H_2O(cr)$ at 25 °C are evaluated from the experimental data of Lokshin et al. [74] at 20 °C and Zambonini and Caglioti [75] at 25 °C, respectively, and for $K_6Nd_4(SO_4)_9{\cdot}8H_2O(cr)$ is evaluated from the experimental data of Zambonini and Caglioti [75] at 25 °C. Those for $NaNd(SO_4)_2{\cdot}H_2O(cr)$ at other temperatures are derived from the experimental data of Schevchuk et al. [77], and those for $KNd(SO_4)_2{\cdot}H_2O(cr)$ at other temperatures are derived from the experimental data of Bunykina et al. [69].

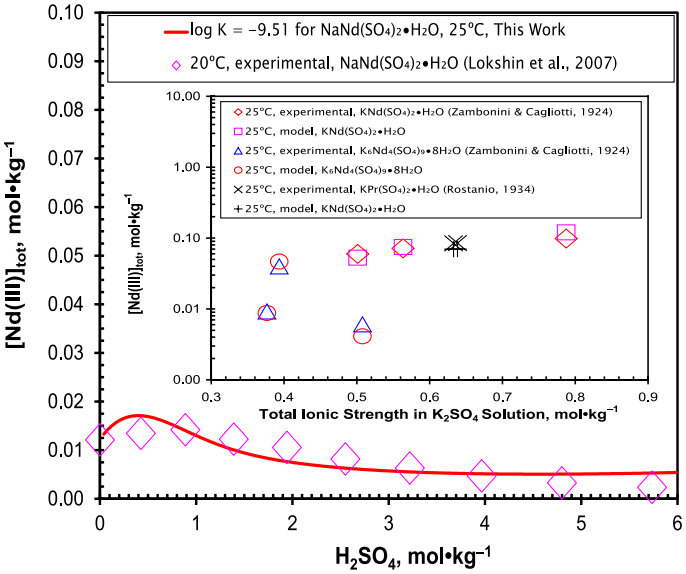


Fig. 6 Solubilities of the double salts of Nd(III) with Na and K in total molality of Nd(III) at 25 °C as a function of concentrations of H_2SO_4 in the main panel and K_2SO_4 in the insert predicted by the model developed in this study in comparison with the respective experimental data at 20 °C and 25 °C. The double salts for the model include $NaNd(SO_4)_2{\cdot}H_2O$, $KNd(SO_4)_2{\cdot}H_2O$, and $K_6Nd_4(SO_4)_9{\cdot}8H_2O$, $KNd(SO_4)_2{\cdot}H_2O$ is used as a homoloque to $KPr(SO_4)_2.H_2O$

using the thermodynamic model established in this study (Table 7). Figure 6 shows the solubilities of $NaNd(SO_4)_2{\cdot}H_2O$(cr) and $KNd(SO_4)_2{\cdot}H_2O$(cr) at 25 °C as a function of concentrations of H_2SO_4 and K_2SO_4 predicted using the $\log_{10} K_{sp}$ obtained in this study, in comparison with the experimental solubility data primarily at 20 °C and 25 °C. The comparison indicates that the predicted values are in good agreement with the experimental data. Notice that the experimental data for $KPr(SO_4)_2{\cdot}H_2O$(cr) at 25 °C from [76] are also plotted in Fig. 6 for the solubilities predicted for $KNd(SO_4)_2{\cdot}H_2O$(cr) based on the model. The comparison is justified because Nd(III) and Pr(III) homologues have very close solubilities in the similar system for $Pr_2(C_2O_4)_3{\cdot}10H_2O$ and

Table 8 Validation test for the solubility constants of alkali and neodymium or praseodymium double sulfate salts on the equilibrium assemblage at 25 °C

Assemblage	$m_{\Sigma Nd \text{ or } \Sigma Pr}$	$m\Sigma SO_4^{2-}$	$m_{Na \text{ or } K}$
$KNd(SO_4)_2{\cdot}H_2O + K_6Nd_4(SO_4)_9{\cdot}8H_2O$[a]	Exp.: 0.0574	Exp.: 0.114	Exp.: 0.0551
	Model: 0.0662	Model: 0.127	Model: 0.0551
$Na_2SO_4{\cdot}10H_2O + NaPr(SO_4)_2{\cdot}H_2O$[b]	Exp.: 0.00855	Exp.: 1.99	Exp.: 3.95
	Model: 0.0128	Model: 2.06	Model: 4.09

[a]The experimental data are from Zambonini and Caglioti [75]. In the calculation, the concentration of potassium is fixed

[b]The experimental data are from Shevchuk and Skorikov [78] for $Na_2SO_4{\cdot}10H_2O + NaPr(SO_4)_2{\cdot}H_2O$. The model-predicted values are for $Na_2SO_4{\cdot}10H_2O + NaNd(SO_4)_2{\cdot}H_2O$, using $NaNd(SO_4)_2{\cdot}H_2O$ as a homologue to $NaPr(SO_4)_2{\cdot}H_2O$

$Nd_2(C_2O_4)_3{\cdot}10H_2O$ [1]. The comparison demonstrates that the model also reproduces the experimental data for $KPr(SO_4)_2{\cdot}H_2O$(cr) in K_2SO_4 solutions well.

The $\log_{10} K_{sp}$ at 50 °C, 75 °C, and 100 °C are obtained by applying the model to the experimental data from [77] for $NaNd(SO_4)_2{\cdot}H_2O$(cr) and from [69] for $KNd(SO_4)_2{\cdot}H_2O$(cr) (Table 7).

In addition, the solubility constant for $K_6Nd_4(SO_4)_9{\cdot}8H_2O$(cr) at 25 °C (Table 7) regarding the following reaction is evaluated from the experimental data of Zambonini and Cagliotti [75] at the same temperature,

$$K_6Nd_4\left(SO_4\right)_9 \cdot 8H_2O(cr) \rightleftharpoons 6K^+ + 4Nd^{3+} + 9SO_4^{2-} + 8H_2O(l) \tag{12}$$

In Table 8, a validation test is performed for the equilibrium constants separately evaluated for $KNd(SO_4)_2{\cdot}H_2O$(cr), $K_6Nd_4(SO_4)_9{\cdot}8H_2O$(cr), and $NaNd(SO_4)_2{\cdot}H_2O$(cr) against the equilibrium compositions for the assemblages of $KNd(SO_4)_2{\cdot}H_2O$(cr) + $K_6Nd_4(SO_4)_9{\cdot}8H_2O$(cr), and $Na_2SO_4{\cdot}10H_2O$ (mirabilite) + $NaPr(SO_4)_2{\cdot}H_2O$(cr). Notice that as mentioned before, Nd(III) and Pr(III) homologues have very close solubilities under the same conditions [1]. Therefore, we use here the assemblage of $Na_2SO_4{\cdot}10H_2O$ + $NaPr(SO_4)_2{\cdot}H_2O$(cr) to represent that of $Na_2SO_4{\cdot}10H_2O$ + $NaNd(SO_4)_2{\cdot}H_2O$(cr). The validation test results indicate that the model-predicted values are in good agreement with the experimental data.

5 Summary

In this work, we have developed a thermodynamic model that can describe the interactions of Nd(III) with sulfate to high ionic strengths up to ~ 16.5 mol·kg^{-1} and from 0 °C to up to 100 °C. Our model is validated by the experimental data that were not used in the model development. The experimental data for the validation tests include the solubility data of Nd-oxalate in H_2SO_4 solutions. The model reproduces the experimental data of Nd-oxalate in H_2SO_4 solutions, validating the interaction parameters in our model that have been established based on the experimental data of $Nd_2(SO_4)_3{\cdot}8H_2O$ in H_2SO_4 solutions. Our model can be applied to many fields, including the extraction of REE and nuclear waste management, and also serves as the benchmark for the future extraction methods that should be environmentally friendlier. The detailed applications to nuclear waste management will be reported elsewhere.

Acknowledgements Sandia National Laboratories (SNL) is a multimission laboratory operated by National Technology and Engineering Solutions of Sandia, LLC., a wholly owned subsidiary of Honeywell International, Inc., for the U.S. Department of Energy's National Nuclear Security Administration under contract DE-NA-0003525. This research is funded by the LDRD from SNL (Project # 222400) and by the Spent Fuel and Waste Science and Technology (SFWST) programs administered by the Office of Nuclear Energy (NE) of the U.S. Department of Energy. This paper describes objective technical results and analysis. Any subjective views or opinions that might be expressed in the paper do not necessarily represent the views of the U.S. Department of Energy or the United States Government. The authors are grateful to the journal reviewers for the detailed and insightful reviews, which led to the significant improvement of our paper. We thank Dr. Luigi Paduano, the Editor, for his time and editorial efforts.

Author Contributions YX wrote the main manuscript, and all authors reviewed and edited the manuscript.

Declarations

Competing interest The authors declare no competing interests.

References

1. Xiong, Y.-L., Wang, Y.-F.: Experimental and modeling studies of Pr and Nd oxalate solubility to high ionic strengths: insight into actinide (III) oxalates. Chem. Geol. **573**, 120200 (2021)
2. Xia, Y.-X., Chen, J.-F., Choppin, G.R.: Solubility, dissociation and complexation with Nd(III) and Th(IV) of oxine, thenoyltrifluoroacetone and 1,10-phenanthronline in 5.0 m NaCl. Talanta **43**, 2073–2081 (1996)
3. Wei, Y.-Z., Sato, N., Nanjo, M.: The solubility of $Sm_2(SO_4)_3$ and $Nd_2(SO_4)_3$ in sulfate solutions: fundamental study on the recycling of rare earth magnet (in Japanese with English abstract). J. Japanese Resour. Mater. Soc. **105**, 965–970 (1989)
4. Todorovsky, D.S., Milanova, M.M., Minkova, N.L., Diakovich, V.A.: The sulfuric acid processing of rare earth concentrate with high calcium content: an attempted simplified mathematical description. Hydrometallurgy **33**, 359–365 (1993)
5. Lokshin, E.P., Vershkova, Y.A., Vershkov, A.V., Tareeva, O.A.: Efficiency of sulphuric acid leaching of lanthanides in relation to quality of phosphosemihydrate obtained from Khibiny apatite concentrate. Russ. J. Appl. Chem. **75**, 1608–1611 (2002)
6. Lebedev, V.N.: Sulfuric acid technology for processing of eudialite concentrate. Russ. J. Appl. Chem. **76**, 1559–1563 (2003)
7. Saito, T., Sato, H., Motegi, T.: Recovery of rare-earth elements. J. Alloy. Compd. **425**, 145–147 (2006)
8. Um, N., Hirato, T.: Dissolution behavior of La_2O_3, Pr_2O_3, Nd_2O_3, CaO and Al_2O_3 in sulfuric acid solutions and study of cerium recovery from rare earth polishing powder waste via two-stage sulfuric acid leaching. Mater. Trans. **54**, 713–719 (2013)
9. Yoon, H.S., Kim, C.J., Chung, K.W., Lee, S.J., Joe, A.R., Shin, Y.H., Lee, S.I., Yoo, S.J., Kim, J.G.: Leaching kinetics of neodymium in sulfuric acid from E-scrap of NdFeB permanent magnet. Korean J. Chem. Eng. **31**, 706–711 (2014)
10. Önal, M.A.R., Borra, C.R., Guo, M., Blanpain, B., Van Gerven, T.: Hydrometallurgical recycling of NdFeB magnets: complete leaching, iron removal and electrolysis. J. Rare Earths **35**, 574–584 (2017)
11. Wang, L., Huang, X., Yu, Y., Zhao, L., Wang, C., Feng, Z., Cui, D., Long, Z.: Towards cleaner production of rare earth elements from bastnaesite in China. J. Clean. Prod. **165**, 231–242 (2017)
12. München, D.D., Bernardes, A.M., Veit, H.M.: Evaluation of neodymium and praseodymium leaching efficiency from post-consumer NdFeB magnets. J. Sustain. Metall. **4**, 288–294 (2018)
13. Chen, S., Huang, X., Feng, Z., Xu, Y., Wang, M., Xia, C., Zhao, L.: Behavior of rare earth, iron, and phosphorus during purification of rare earth sulfate leach solution using magnesium oxide. Hydrometallurgy **196**, 105377 (2020)
14. Zhou, Y., Liu, J., Cheng, G., Xue, X., Yang, H.: Carbothermal reduction followed by sulfuric acid leaching of Bayan Obo tailings for selective concentration of iron and rare earth metals. Sep. Purif. Technol. **271**, 118742 (2021)
15. Tian, J., Yin, J.-Q., Chi, R., Rao, G.-H., Jiang, M.-T., Ouyang, K.-X.: Kinetics on leaching rare earth from the weathered crust elution-deposited rare earth ores with ammonium sulfate solution. Hydrometallurgy **101**, 166–170 (2010)
16. Xiao, Y.-F., Feng, Z.-Y., Huang, X.-W., Huang, L., Chen, Y.-Y., Wang, L.-S., Long, Z.-Q.: Recovery of rare earths from weathered crust elution-deposited rare earth ore without ammonia-nitrogen pollution: I leaching with magnesium sulfate. Hydrometallurgy **153**, 58–65 (2015)
17. Su, X., Wang, Y., Su, J., Lai, W., Gao, Y., Sun, X.: Enrichment of rare earths in magnesium sulfate leach solutions of ion-absorbed ores by extraction-precipitation. Hydrometallurgy **189**, 105119 (2019)
18. Xin, W., Deng, Y., Jiang, Y., Zhang, J., Chen, D.: Sulfurization roasting process of Nd_2O_3 and synthetic $NdFeO_3$ with ferric sulfate. Metall. Mater. Trans. B **52**, 1–12 (2021)
19. Um, N., Hirato, T.: Precipitation of cerium sulfate converted from cerium oxide in sulfuric acid solutions and the conversion kinetics. Mater. Trans. **53**, 1986–1991 (2012)
20. Takahashi, T., Takano, A., Saitoh, T., Nagano, N., Hirai, S., Shimakage, K.: Separation and recovery of rare earth elements from phosphor sludge in processing plant of waste fluorescent lamp by pneumatic classification and sulfuric acidic leaching (in Japanese with English abstract). Resour. Raw Mater. **117**, 579–585 (2001)
21. Korkmaz, K., Alemrajabi, M., Rasmuson, Å., Forsberg, K.: Recoveries of valuable metals from spent nickel metal hydride vehicle batteries via sulfation, selective roasting, and water leaching. J. Sustain. Metall. **4**, 313–325 (2018)
22. Zielinski, M., Cassayre, L., Destrac, P., Coppey, N., Garin, G., Biscans, B.: Leaching mechanisms of industrial powders of spent nickel metal hydride batteries in a pilot-scale reactor. Chemsuschem **13**, 616–628 (2020)

23. Guerrero, A., Hernández, M.S., Goñi, S.: Effect of simulated radioactive liquid waste on the microstructure of cementitious materials: portlandite orientation and saturation factors in the pore solution. J. Am. Ceram. Soc. **83**, 2803–2808 (2000)
24. Xiong, Y.-L., Lord, A.S.: Experimental investigations of the reaction path in the $MgO–H_2O–CO_2$ system in solutions with various ionic strengths, and their applications to nuclear waste isolation. Appl. Geochem. **23**, 1634–1659 (2008)
25. Xiong, Y.-L., Kirkes, L., Marrs, C.: Experimental determination of solubility of neodymium hydroxide in Na_2SO_4 solutions to high ionic strength at 298.15 K under well-constrained conditions: applications to nuclear waste isolation. East Asia Forum on Radwaste Management (EAFORM), October 25–28, 2015, Taichung, Taiwan, R.O.C. SAND2015–9185C (2015)
26. Xiong, Y.-L., Kirkes, L., Marrs, C.: A Pitzer Model for $Na^+–Nd^{3+}–SO_4^{2-}–H^+–OH^-$ system to high ionic strengths. Geological society of America annual meeting, September 25–28, 2016, Denver, CO, USA. SAND2016–9407C (2016)
27. Xiong, Y.-L., Kirkes, L., Knox, J., Marrs, C., Dean, J.: Am(III)/Nd(III)—sulfate interactions at elevated temperatures in high ionic strength environments. ThermAc Workshop on aquatic actinide chemistry andthermodynamics at elevated temperatures, Dec 1–2, 2016, Dresden, Germany. SAND2016–11849C (2016)
28. Sun, H.-F., Zhao, F.-H., Zhang, M., Li, J.-Q.: Behavior of rare earth elements in acid coal mine drainage in Shanxi Province, China. Environ. Earth Sci. **67**, 205–213 (2012)
29. Prudêncio, M.I., Valente, T., Marques, R., Braga, M.A.S., Pamplona, J.: Geochemistry of rare earth elements in a passive treatment system built for acid mine drainage remediation. Chemosphere **138**, 691–700 (2015)
30. Li, X.-X., Wu, P.: Geochemical characteristics of dissolved rare earth elements in acid mine drainage from abandoned high-As coal mining area, southwestern China. Environ. Sci. Pollut. Res. **24**, 20540–20555 (2017)
31. Migaszewski, Z.M., Gałuszka, A., Dołęgowska, S.: Extreme enrichment of arsenic and rare earth elements in acid mine drainage: case study of Wiśniówka mining area (south-central Poland). Environ. Pollut. **244**, 898–906 (2019)
32. Wei, X.-C., Zhang, S.-C., Shimko, J., Dengler, R.W., II.: Mine drainage: treatment technologies and rare earth mine drainage: treatment technologies and rare earth. Water Environ. Res. **91**, 1061–1068 (2019)
33. Wolery, T.J., Xiong, Y.-L., Long, J.: Verification and validation plan/validation document for EQ3/6 version 8.0a for actinide chemistry, document version 8.10. Carlsbad, NM: Sandia National Laboratories. ERMS550239 (2010)
34. Xiong, Y.-L.: WIPP verification and validation plan/validation document for EQ3/6 version 8.0a for actinide chemistry, revision 1, document version 8.20. Supersedes ERMS550239. Carlsbad, NM: Sandia National Laboratories. ERMS555358 (2011)
35. Xiong, Y.-L.: An aqueous thermodynamic model for solubility of potassium ferrate in alkaline solutions to high ionic strengths at 283.15 K to 333.15 K. J. Solution Chem. **42**, 1393–1403 (2013)
36. Xiong, Y.-L.: A thermodynamic model for silica and aluminum in alkaline solutions with high ionic strength at elevated temperatures up to 100°C: applications to zeolites. Am. Miner. **98**, 141–153 (2013)
37. Xiong, Y.-L.: A Pitzer model for the $Na\text{-}Al(OH)_4\text{-}Cl\text{-}OH$ system and solubility of boehmite (AlOOH) to high ionic strength and to 250°C. Chem. Geol. **373**, 37–49 (2014)
38. Domski, P.S.: "Memo AP-173, EQ3/6 database update: DATA0.FM2" memorandum to WIPP Records, October 27, 2015. Carlsbad, NM: Sandia National Laboratories. ERMS564914 (2015)
39. Domski, P.S., Xiong, Y.-L.: Prediction of baseline actinide solubilities with an updated EQ3/6 thermodynamic database (DATA0.FM2) in response EPA completeness comment 3-C-3 for CRA2014. Carlsbad, NM: Sandia National Laboratories. ERMS565032 (2015)
40. Xiong, Y.-L., Domski, P.S.: Updating the WIPP thermodynamic database, revision 1, supersedes ERMS565730. Carlsbad, NM: Sandia National Laboratories. ERMS566047(2016)
41. Harvie, C.E., Møller, N., Weare, J.H.: The prediction of mineral solubilities in natural waters: the $Na\text{-}K\text{-}Mg\text{-}Ca\text{-}H\text{-}Cl\text{-}SO_4\text{-}OH\text{-}HCO_3\text{-}CO_3\text{-}CO_2\text{-}H_2O$ system to high ionic strengths at 25°C. Geochim. Cosmochim. Acta **48**, 723–751 (1984)
42. Wolery, T., Jove-Colon, C., Rard, J., Wijesinghe, A.: Pitzer database development: description of the Pitzer geochemical thermodynamic database data0. ypf. Appendix I in in-drift precipitates/salts model (P. Mariner) Report ANL-EBS-MD-000045 REV, 2 (2004)
43. Truesdell, A.H., Hostetler, P.B.: Dissociation constants of KSO_4^- from 10°–50°C. Geochim. Cosmochim. Acta **32**, 1019–1022 (1968)

44. Pokrovski, G.S., Schott, J., Sergeyev, A.S.: Experimental determination of the stability constants of $NaSO_4^-$ and $NaB(OH)_4^0$ in hydrothermal solutions using a new high-temperature sodium-selective glass electrode—implications for boron isotopic fractionation. Chem. Geol. **124**, 253–265 (1995)
45. Holmes, H.F., Mesmer, R.E.: An isopiestic study of $\{(1-y)NaHSO_4 + yNa_2SO_4\}(aq)$ at elevated temperatures. J. Chem. Thermodyn. **26**, 581–594 (1994)
46. Wang, M., Zhang, Y., Muhammed, M.: Critical evaluation of thermodynamics of complex formation of metal ions in aqueous solutions I: a description of evaluation methods. Hydrometallurgy **45**, 21–36 (1997)
47. Xiong, Y.-L.: Estimation of medium effects on equilibrium constants in moderate and high ionic strength solutions at elevated temperatures by using specific interaction theory (SIT): interaction coefficients involving Cl^-, OH^- and Ac^- up to 200 °C and 400 bars. Geochem. Trans. **7**, 4 (2006). https://doi.org/10.1186/1467-4866-7-4
48. Wolery, T.W., Jarek, R.L.: Software user's manual. EQ3/6, version, 8. Software Document, (10813-UM), p.376 (2003)
49. Wolery, T.W., Sutton, M.: Generic natural systems evaluation-thermodynamic database development and data management (No. LLNL-TR-500113). Lawrence Livermore National Lab (LLNL), Livermore, CA (United States) (2011)
50. Gu, Y., Gammons, C.H., Bloom, M.S.: A one-term extrapolation method for estimating equilibrium constants of aqueous reactions at elevated temperatures. Geochim. Cosmochim. Acta **58**, 3545–3560 (1994)
51. Ridley, M.K., Wesolowski, D.J., Palmer, D.A., Kettler, R.M.: Association quotients of aluminum sulphate complexes in NaCl media from 50 to 125°C: results of a potentiometric and solubility study. Geochim. Cosmochim. Acta **63**, 459–472 (1999)
52. Xiao, C., Wesolowski, D.J., Palmer, D.A.: Formation quotients of aluminum sulfate complexes in $NaCF_3SO_3$ media at 10, 25, and 50°C from potentiometric titrations using a mercury/mercurous sulfate electrode concentration cell. Environ. Sci. Technol. **36**, 166–173 (2002)
53. Wood, S.A.: The aqueous geochemistry of the rare-earth elements and yttrium: 1. Review of available low-temperature data for inorganic complexes and the inorganic REE speciation of natural waters. Chem. Geol. **82**, 159–186 (1990)
54. Wood, S.A.: The aqueous geochemistry of the rare-earth elements and yttrium: 2. Theoretical predictions of speciation in hydrothermal solutions to 350°C at saturation water vapor pressure. Chem. Geol. **88**, 99–125 (1990)
55. Migdisov, A.A., Reukov, V.V., Williams-Jones, A.E.: A spectrophotometric study of neodymium (III) complexation in sulfate solutions at elevated temperatures. Geochim. Cosmochim. Acta **70**, 983–992 (2006)
56. Migdisov, A.A., Williams-Jones, A.E.: A spectrophotometric study of Nd (III), Sm (III) and Er (III) complexation in sulfate-bearing solutions at elevated temperatures. Geochim. Cosmochim. Acta **72**, 5291–5303 (2008)
57. Fanghänel, T., Kim, J.I.: Spectroscopic evaluation of thermodynamics of trivalent actinides in brines. J. Alloy. Compd. **271**, 728–737 (1998)
58. Neck, V., Fanghänel, T., Kim, J.I.: Aquatic chemistry and thermodynamic modelling of trivalent actinides (No. FZKA-6110). Forschungszentrum Karlsruhe GmbH Technik und Umwelt (Germany). Inst. fuer Nukleare Entsorgungstechnik (1998)
59. Rai, D., Felmy, A.R., Fulton, R.W.: Nd^{3+} and Am^{3+} ion interactions with sulfate ion and their influence on $NdPO_4(c)$ solubility. J. Solution Chem. **24**, 879–895 (1995)
60. Das, G., Lencka, M.M., Eslamimanesh, A., Wang, P., Anderko, A., Riman, R.E., Navrotsky, A.: Rare earth sulfates in aqueous systems: thermodynamic modeling of binary and multicomponent systems over wide concentration and temperature ranges. J. Chem. Thermodyn. **131**, 49–79 (2019)
61. Vercouter, T., Amekraz, B., Moulin, C., Giffaut, E., Vitorge, P.: Sulfate complexation of trivalent lanthanides probed by nanoelectrospray mass spectrometry and time-resolved laser-induced luminescence. Inorg. Chem. **44**, 7570–7581 (2005)
62. Skerencak, A., Panak, P.J., Fanghänel, T.: Complexation and thermodynamics of Cm (III) at high temperatures: the formation of $[Cm(SO_4)_n]^{3-2n}$ ($n = 1, 2, 3$) complexes at $T = 25$ to 200°C. Dalton Trans. **42**, 542–549 (2013)
63. Choppin, G.R., Bond, A.H., Borkowski, M., Bronikowski, M.G., Chen, J.-F., Lis, S., Mizera, J., Pokrovsky, O.S., Wall, N.A., Xia, Y.-X., Moore, R.C.: Waste isolation pilot plant actinide source term test program: solubility studies and development of modeling parameters. Sandia National Laboratories Report. SAND99–0943 (2001)

64. Friend, J.A.N.: The solubility of neodymium sulphate in water and in sulphuric acid solutions at various temperatures: a new hydrate. J. Chem. Soc. (Resumed) (1930). https://doi.org/10.1039/JR9300001633
65. Kirmse, E.M., Schüchner, G.: Loslichkeit von Seltenerdsulfaten in Schwefelsiiure (Solubility of rare earth sulfates in sulfuric acid). Zeitschmift fur Chemie **27**, 267–268 (1987)
66. Rard, J.A.: Aqueous solubilities of praseodymium, europium and lutetium sulphates. J. Solution Chem. **17**, 499–517 (1988)
67. Todorovsky, D.S., Milanova, M.M., Minkova, N.L., Balarev, C.: Solubility of some lanthanide sulfates in polycomponent systems containing H_2SO_4. Monatshefte für Chemie/Chem. Monthly **124**, 673–679 (1993)
68. Bunyakina, N.V., Storozhenko, D.A.: $MgSO_4$–$Ln_2(SO_4)_3$–H_2O (Ln= Pr, Nd, Gd) systems at 25°C. Russ. J. Inorg. Chem. **49**(11), 1772–1774 (2004)
69. Bunyakina, N.V., Storozhenko, D.A., Shevchuk, V.G.: Phase Equilibria in the M_2SO_4–$Nd_2(SO_4)3_H_2O$ (M = K, NH_4) systems at 50–100°C. Russ. J. Inorg. Chem. **35**, 570–572 (1990)
70. Thakur, P., Xiong, Y., Borkowski, M.: An improved thermodynamic model for the complexation of trivalent actinides and lanthanide with oxalic acid valid to high ionic strength. Chem. Geol. **413**, 7–17 (2015)
71. Sarver, L.A., Brinton, P.H.P.: The solubilities of some rare-earth oxalates. J. Am. Chem. Soc. **49**, 943–958 (1927)
72. Kul, M., Topkaya, Y., Karakaya, I.: Rare earth double sulfates from pre-concentrated bastnasite. Hydrometallurgy **93**, 129–135 (2008)
73. Porvali, A., Wilson, B.P., Lundström, M.: Lanthanide-alkali double sulfate precipitation from strong sulfuric acid NiMH battery waste leachate. Waste Manage. **71**, 381–389 (2018)
74. Lokshin, E.P., Tareeva, O.A., Kashulina, T.G.: A study of the solubility of yttrium, praseodymium, neodymium and gadolinium sulphates in the presence of sodium and potassium in sulphuric-phosphoric acid solutions at 20°C. Russ. J. Appl. Chem. **80**, 1275–1280 (2007)
75. Zambonini, F., Cagliotti, V.: Rare earth and alkali metal double sulfates: II. Sulfates of neodymium and potassium. Atti della Accademia Nazionale dei Lincei **5**, 308–313 (1924)
76. Restaino, S.: The double sulphates of rare earths and alkali metals: praseodymium and potassium sulphates. Atti della Accademia Nazionale dei Lincei **20**, 192–200 (1934)
77. Shevchuk, V.G.; Storozhenko, D.A.; Bunyakina, N.V.: Solubility in NaA–NdA–H_2O (A=Cl, SO_4) systems at 50, 75, and 100°C. Zhurnal Neorganicheskoi Khimii (Russ. J. Inorg. Chem.), 1063–1064 (1988)
78. Shevchuk, A.V., Skorikov, V.M.: Ternary aqueous systems of praseodymium and alkali metal sulfate salts at 25°C. Zhurnal Neorganicheskoi Khimii **25**, 1121–1124 (1980)

Publisher's Note Springer Nature remains neutral with regard to jurisdictional claims in published maps and institutional affiliations.

Springer Nature or its licensor (e.g. a society or other partner) holds exclusive rights to this article under a publishing agreement with the author(s) or other rightsholder(s); author self-archiving of the accepted manuscript version of this article is solely governed by the terms of such publishing agreement and applicable law.